Journal of Hydrology 558 (2018) 496–508

Contents lists available at ScienceDirect

Journal of Hydrology

journal homepage: www.elsevier.com/locate/jhydrol

Research papers

An approximate analytical solution for describing surface runoff and sediment transport over hillslope

Wanghai Tao [a], Quanjiu Wang [a,b,*], Henry Lin [a,c,d]

[a] State Key Laboratory Base of Eco-hydraulic Engineering in Arid Area, Xi'an University of Technology, Xi'an 710048, China
[b] State Key Laboratory of Soil Erosion and Dryland Farming on the Loess Plateau, Institute of Soil and Water Conservation, Northwest A & F University, Xi'an 712100, China
[c] State Key Laboratory of Loess and Quaternary Geology, Institute of Earth Environment, Chinese Academy of Sciences, Xi'an, China
[d] Department of Ecosystem Science and Management, The Pennsylvania State University, University Park, PA 16802, USA

ARTICLE INFO

Article history:
Received 6 July 2017
Received in revised form 14 November 2017
Accepted 25 January 2018
Available online 3 February 2018
This manuscript was handled by Marco Borga, Editor-in-Chief, with the assistance of Jennifer Guohong Duan, Associate Editor

Keywords:
Overland flow
Soil erosion
Approximate analytical solution
Natural rainfall

ABSTRACT

Soil and water loss from farmland causes land degradation and water pollution, thus continued efforts are needed to establish mathematical model for quantitative analysis of relevant processes and mechanisms. In this study, an approximate analytical solution has been developed for overland flow model and sediment transport model, offering a simple and effective means to predict overland flow and erosion under natural rainfall conditions. In the overland flow model, the flow regime was considered to be transitional with the value of parameter β (in the kinematic wave model) approximately two. The change rate of unit discharge with distance was assumed to be constant and equal to the runoff rate at the outlet of the plane. The excess rainfall was considered to be constant under uniform rainfall conditions. The overland flow model developed can be further applied to natural rainfall conditions by treating excess rainfall intensity as constant over a small time interval. For the sediment model, the recommended values of the runoff erosion calibration constant (c_r) and the splash erosion calibration constant (c_f) have been given in this study so that it is easier to use the model. These recommended values are 0.15 and 0.12, respectively. Comparisons with observed results were carried out to validate the proposed analytical solution. The results showed that the approximate analytical solution developed in this paper closely matches the observed data, thus providing an alternative method of predicting runoff generation and sediment yield, and offering a more convenient method of analyzing the quantitative relationships between variables. Furthermore, the model developed in this study can be used as a theoretical basis for developing runoff and erosion control methods.

1. Introduction

Soil erosion and nutrient loss caused by rainfall contribute significantly to land degradation and nonpoint source pollution. The processes of runoff generation and soil erosion need to be better understood and quantified. Predicting rainfall runoff is critical in predicting soil erosion (Raff and Ramirez, 2005). Mathematical models related to runoff generation and sediment transport have been used as an effective way of predicting soil and water loss during rainfall, with the process of overland flow generation usually described using Saint-Venant equations (i.e., the continuity equation and the momentum equation) (Wang et al., 2002). However, it is very difficult to obtain analytical solutions as these equations are highly nonlinear (Wang et al., 2006), meaning that only numerical techniques can be used (Ying et al., 2004; Crossley et al., 2003; Lackey and Sotiropoulos, 2005). When the acceleration term is ignored, the Saint-Venant equations can be simplified using diffusion wave equations. Hayami (1951) developed an analytical solution for diffusion wave equations (in rivers) by using a disturbance function; Kazeyilmaz-Ahan and Medina (2007) and Kazeyilmaz-Ahan (2012) provided a solution for overland flow, then improved the solution for diffusion waves applied to overland flow by employing the De Hoog algorithm. Govindaraju et al. (1988) and Rao and Kavvas (1991) suggested that diffusion wave equations may be better suited to steep rough slopes. When the acceleration and pressure terms are ignored, the Saint-Venant equations can be expressed as kinematic wave equations. The explicit analytical solution (for uniform rainfall in time and space) to kinematic wave equations was first given by Henderson and Wooding (1964). Parlange et al. (1981) developed a general analytical solution to the kinematic flow for variable rainfall. Sander et al. (1990) obtained the solution for when infiltration rate exceeds rainfall

* Corresponding author at: State Key Laboratory Base of Eco-hydraulic Engineering in Arid Area, Xi'an University of Technology, Xi'an 710048, China.
E-mail address: wquanjiu@163.com (Q. Wang).

https://doi.org/10.1016/j.jhydrol.2018.01.054
0022-1694/

intensity by considering the excess rainfall to be equal to the hydraulic conductivity. Luce and Cundy (1992) modified the kinematic wave equation by using the Philips infiltration equation to predict excess rainfall, and applied the solution to field data. Tsai and Yang (2005) used the method of characteristics integrated with cubic spline interpolation to compute one-dimensional and two-dimensional kinematic wave models. To obtain the closed form of the analytical solution, Mizumura (2006) assumed that the unit discharge in Manning's formula was a parabolic curve. Gottardi and Venutelli (2008) suggested an accurate time integration method for diffusion wave and kinematic wave equations. Morooka et al. (2016) proposed a new theoretical framework (theory of stochastic process) to estimate rainfall runoff.

Foster (1986) defined detachment as the soil particles being removed from the soil surface and transport as the detached soil particles moving to some location away from the detachment point. The processes of detachment and transport can be described using the continuity equation, with sediment discharge considered to be a function of water flow, soil properties, and topography (Bennet, 1974). Most of the physical model developed in this study was based on the continuity equation. The ANSWERS (Areal Nonpoint Source Watershed Response Simulation) model was used to predict erosion of agricultural watersheds by treating runoff and erosion as independent processes (Beasley et al., 1980). The WEEP (Water Erosion Prediction Project) model (Nearing et al., 1989) divides rainfall erosion into rill and interrill areas, and calculates the erosion in these areas separately. EUROSEM (Euro Open Soil Erosion Model) (Morgan et al., 1998) is an event-based model which assumes that a few events every year are the main contributors to erosion; it also calculates rill erosion and interrill erosion separately.

For this paper, an approximate analytical model for predicting overland flow and rainfall erosion was developed. The overland flow model was then used to predict flow and erosion under natural rainfall conditions. The recommended values for the runoff erosion calibration and splash erosion calibration constants are defined in this paper, producing a simple and effective model for predicting overland flow and erosion under natural rainfall conditions.

2. Theoretical analysis

2.1. Overland flow

The kinematic wave model was used to describe the process of overland flow generation:

$$\frac{\partial Q(x,t)}{\partial x}+\frac{\partial h(x,t)}{\partial t}=r_e(t) \tag{1}$$

$$Q(x,t)=\alpha h(x,t)^{\beta} \tag{2}$$

where $Q(x, t)$ is the unit discharge (cm^2/min), $h(x, t)$ is the depth of overland flow (cm), x is the distance along the overland plane (cm), t is rainfall duration (min), r_e is excess rainfall (cm/min), $\alpha = J^{1/2}/n$ ($cm^{1/3}$/min), J is the overland slope (cm/cm), n is Manning's roughness coefficient (min/$cm^{1/3}$), and β is an exponent that reflects the degree of turbulence ($5/3 < \beta < 3$) (Emmett, 1970; Sander et al., 2014).

Assuming that the change rate of unit discharge with distance is constant, and also equals the discharge per unit area at the outlet of the plane (Moore, 1985; Agnese et al., 2001), the unit discharge can be expressed as:

$$Q(x,t)=q(t)x \tag{3}$$

where $q(t)$ is the discharge per unit area (cm/min).

Combining Eqs. (2) and (3) yields the depth of the overland flow:

$$h(x,t)=\left(\frac{x}{\alpha}q(t)\right)^{\frac{1}{\beta}} \tag{4}$$

Differentiating Eq. (4) yields the change rate of flow depth with time:

$$\frac{\partial h(x,t)}{\partial t}=\frac{1}{\beta}\left(\frac{x}{\alpha}\right)^{\frac{1}{\beta}}q(t)^{\frac{1-\beta}{\beta}}\frac{dq(t)}{dt} \tag{5}$$

Substituting Eq. (5) into Eq. (1) gives:

$$q(t)+\frac{1}{\beta}\left(\frac{x}{\alpha}\right)^{\frac{1}{\beta}}q(t)^{\frac{1-\beta}{\beta}}\frac{dq(t)}{dt}=r_e(t) \tag{6}$$

Integrating both sides of Eq. (6) with respect to distance x (from 0 to L) gives:

$$\int_0^L r_e(t)dx-\int_0^L q(t)dx=\frac{1}{\beta}q(t)^{\frac{1-\beta}{\beta}}\frac{dq(t)}{dt}\int_0^L\left(\frac{x}{\alpha}\right)^{\frac{1}{\beta}}dx \tag{7}$$

The result of the integration is:

$$r_e(t)L-q(t)L=q(t)^{\frac{1-\beta}{\beta}}\frac{dq(t)}{dt}\frac{L}{1+\beta}\left(\frac{L}{\alpha}\right)^{1/\beta} \tag{8}$$

Separating variables $q(t)$ and t, we obtain:

$$dt=\frac{q(t)^{\frac{1-\beta}{\beta}}}{r_e(t)-q(t)}\frac{1}{\beta+1}\left(\frac{L}{\alpha}\right)^{1/\beta}dq(t) \tag{9}$$

Integrating Eq. (9):

$$t-t_p=\frac{\left(\frac{L}{\alpha}\right)^{\frac{1}{\beta}}}{(\beta+1)}\int\frac{q(t)^{\frac{1-\beta}{\beta}}}{r_e(t)-q(t)}dq(t) \tag{10}$$

where t_p is the time of ponding (min).

2.1.1. The approximate solution under uniform rainfall conditions

Most of the rainfall experiments were carried out under uniform rainfall conditions. In order to obtain an approximate solution under uniform rainfall conditions, it is necessary to estimate accurately the parameters, particularly β, which reflects the degree of turbulence and the type of flow regime that the overland flow belongs to. In this research, the flow regime is treated as transitional, with the value of β approximated to be two (Horton, 1938; Agnese et al., 2001; Singh, 2002). In addition, the excess rainfall under uniform rainfall intensity conditions was considered to be a constant (i.e., rainfall intensity minus stable infiltration rate) when obtaining the solution to the integration of Eq. (10) (Agnese et al., 2001; Moore, 1985). Then, Eq. (10) can be approximated as:

$$t-t_p=\frac{1}{3}\left(\frac{L}{\alpha}\right)^{\frac{1}{2}}\int_{q(t_p)}^{q(t)}\frac{q(t)^{-\frac{1}{2}}}{r_e-q(t)}dq(t) \tag{11}$$

Hence, for uniform rainfall intensity, the outflow rate in the rising stage can be expressed as:

$$q(t)=\tanh^2\left(\frac{3}{2}\sqrt{\frac{\alpha r_e}{L}}(t-t_p)\right)r_e \tag{12}$$

The unit discharge and flow depth in the rising stage can be expressed as:

$$Q(x,t)=\tanh^2\left(\frac{3}{2}\sqrt{\frac{\alpha r_e}{L}}(t-t_p)\right)r_e x \tag{13}$$

$$h(x,t)=\sqrt{\frac{r_e x}{\alpha}}\tanh\left(\frac{3}{2}\sqrt{\frac{\alpha r_e}{L}}(t-t_p)\right) \tag{14}$$

The recession stage begins when rainfall ends (i.e., $r_e = 0$). Eq. (11) can then be expressed as:

$$t - t_s = -\frac{1}{3}\left(\frac{L}{\alpha}\right)^{\frac{1}{2}} \int_{q(t_s)}^{q(t)} q(t)^{-\frac{3}{2}} dq(t) \tag{15}$$

where t_s is the time when the rainfall stops (min), $q(t_s)$ is the discharge per unit area when rainfall stops (cm/min).

Hence, the outflow rate in the recession stage can be expressed as:

$$q_r(t) = q(t_s)\left(1 + \frac{3}{2}(t - t_s)\sqrt{\frac{\alpha q(t_s)}{L}}\right)^{-2} \tag{16}$$

where $q_r(t)$ is the discharge per unit area in the recession stage.

The unit discharge and water depth in the recession stage can be expressed as:

$$Q_r(x,t) = q(t_s)\left(1 + \frac{3}{2}(t - t_s)\sqrt{\frac{\alpha q(t_s)}{L}}\right)^{-2} x \tag{17}$$

$$h_r(x,t) = \sqrt{\frac{x q(t_s)}{\alpha}}\left(1 + \frac{3}{2}(t - t_s)\sqrt{\frac{\alpha q(t_s)}{L}}\right)^{-1} \tag{18}$$

where $Q_r(x, t)$ is the unit discharge (cm^2/min), and $h_r(x, t)$ is the runoff depth (cm) in the recession stage.

Integrating Eqs. (12) and (16) with respect to t yields the total runoff:

$$R(t) = r_e(t - t_p) - \frac{4}{3}\sqrt{\frac{Lr_e}{\alpha}}\left(\exp^2\left(-\frac{3}{2}\sqrt{\frac{\alpha r_e}{L}}(t - t_p)\right) + 1\right)^{-1} + \frac{2}{3}\sqrt{\frac{Lr_e}{\alpha}} \quad t \leqslant t_s \tag{19a}$$

$$R(t) = r_e(t_s - t_p) - \frac{4}{3}\sqrt{\frac{Lr_e}{\alpha}}\left(\exp^2\left(-\frac{3}{2}\sqrt{\frac{\alpha r_e}{L}}(t_s - t_p)\right) + 1\right)^{-1} + \frac{2}{3}\sqrt{\frac{Lr_e}{\alpha}} - \frac{\frac{4}{9}\sqrt{\frac{q(t_s)L}{\alpha}}}{\sqrt{\frac{\alpha q(t_s)}{L}}(t - t_s) + \frac{2}{3}} + \frac{2}{3}\sqrt{\frac{q(t_s)L}{\alpha}} \quad t > t_s \tag{19b}$$

where $R(t)$ is the total runoff in a rainfall event (cm).

Using the parameters shown in Table 1, the unit discharge on the slope was simulated for three rainfall intensities, three slope lengths and three values of parameter α (Examples A, B and C). Fig. 1 shows the calculated results (using Eq. (17)) for unit discharge. The simulated results show that the analytical solutions have a good performance in describing the processes of runoff generation. Note that the increasing values of α results in an increased unit discharge. The values of α are affected by slope gradient and the roughness coefficient. Therefore, Fig. 1C shows the comprehensive effects of slope gradients and roughness coefficients.

2.1.2. The approximate solution under natural rainfall conditions

The natural rainfall process does not result in absolutely uniform rainfall intensity. Thus, the application of the approximate solution under natural rainfall conditions needs to be further analyzed. The natural rainfall process can be divided into several events based on the rainfall intensity. Assuming $q(t_0) = q_0$ (t_0 is any time during the rainfall event), the excess rainfall can be considered constant over a small time interval $[t_0, t]$. There are then some different cases to be examined.

Case 1: $r_e > q_0$. In this case, the integration of Eq. (10) gives:

$$t - t_0 = \frac{2}{3}\sqrt{\frac{L}{\alpha r_e}}\left(\operatorname{arctanh}\left(\sqrt{\frac{q(t)}{r_e}}\right) - \operatorname{arctanh}\left(\sqrt{\frac{q_0}{r_e}}\right)\right) \tag{20}$$

The solution of Eq. (20) is:

$$q(t) = \tanh^2\left(\operatorname{arctanh}\left(\sqrt{\frac{q_0}{r_e}}\right) + \frac{3}{2}\sqrt{\frac{\alpha r_e}{L}}(t - t_0)\right) r_e \tag{21}$$

The unit discharge, flow depth and the runoff amount under Case 1 condition can be expressed as:

$$Q(x,t) = \tanh^2\left(\operatorname{arctanh}\left(\sqrt{\frac{q_0}{r_e}}\right) + \frac{3}{2}\sqrt{\frac{\alpha r_e}{L}}(t - t_0)\right) r_e x \tag{22}$$

$$h(x,t) = \sqrt{\frac{r_e x}{\alpha}}\tanh\left(\operatorname{arctanh}\left(\sqrt{\frac{q_0}{r_e}}\right) + \frac{3}{2}\sqrt{\frac{\alpha r_e}{L}}(t - t_0)\right) \tag{23}$$

$$R(t) = r_e(t - t_0) - \frac{4}{3} \times \sqrt{\frac{Lr_e}{\alpha}}\left(\exp^2\left(-\operatorname{arctanh}\left(\sqrt{\frac{q_0}{r_e}}\right) - \frac{3}{2}\sqrt{\frac{\alpha r_e}{L}}(t - t_0)\right) + 1\right)^{-1} + \frac{4}{3}\sqrt{\frac{Lr_e}{\alpha}}\left(\exp^2\left(-\operatorname{arctanh}\left(\sqrt{\frac{q_0}{r_e}}\right)\right) + 1\right)^{-1} \tag{24}$$

Case 2: $0 < r_e < q_0$. In this case the integration of Eq. (9) gives:

$$t - t_0 = \frac{2}{3}\sqrt{\frac{L}{\alpha r_e}}\left(\operatorname{arccoth}\left(\sqrt{\frac{q(t)}{r_e}}\right) - \operatorname{arccoth}\left(\sqrt{\frac{q_0}{r_e}}\right)\right) \tag{25}$$

The solution of Eq. (25) is:

$$q(t) = \coth^2\left(\operatorname{arccoth}\left(\sqrt{\frac{q_0}{r_e}}\right) + \frac{3}{2}\sqrt{\frac{\alpha r_e}{L}}(t - t_0)\right) r_e \tag{26}$$

The unit discharge, flow depth and the runoff amount under Case 2 condition can be expressed as:

$$Q(x,t) = \coth^2\left(\operatorname{arccoth}\left(\sqrt{\frac{q_0}{r_e}}\right) + \frac{3}{2}\sqrt{\frac{\alpha r_e}{L}}(t - t_0)\right) r_e x \tag{27}$$

$$h(x,t) = \sqrt{\frac{r_e x}{\alpha}}\coth\left(\operatorname{arccoth}\left(\sqrt{\frac{q_0}{r_e}}\right) + \frac{3}{2}\sqrt{\frac{\alpha r_e}{L}}(t - t_0)\right) \tag{28}$$

$$R(t) = r_e(t - t_0) + \frac{4}{3} \times \sqrt{\frac{Lr_e}{\alpha}}\left(\exp^2\left(-\operatorname{arccoth}\left(\sqrt{\frac{q_0}{r_e}}\right) - \frac{3}{2}\sqrt{\frac{\alpha r_e}{L}}(t - t_0)\right) - 1\right)^{-1} - \frac{4}{3}\sqrt{\frac{Lr_e}{\alpha}}\left(\exp^2\left(-\operatorname{arccoth}\left(\sqrt{\frac{q_0}{r_e}}\right)\right) - 1\right)^{-1} \tag{29}$$

Case 3: $r_e = 0$. In this case the integration of Eq. (9) gives:

$$t - t_0 = \frac{1}{3}\sqrt{\frac{L}{\alpha}}\left(\frac{2}{\sqrt{q(t)}} - \frac{2}{\sqrt{q_0}}\right) \tag{30}$$

Table 1
Parameters used in the analytical solution under uniform rainfall conditions.

Parameters	Example A	Example B	Example C
r_e (cm/min)	0.05, 0.1 and 0.15	0.1	0.1
L (cm)	1000	500, 1000 and 1500	1000
α	100	100	50, 100 and 150
t_s (min)	30	30	30
t_p (min)	1	1	1

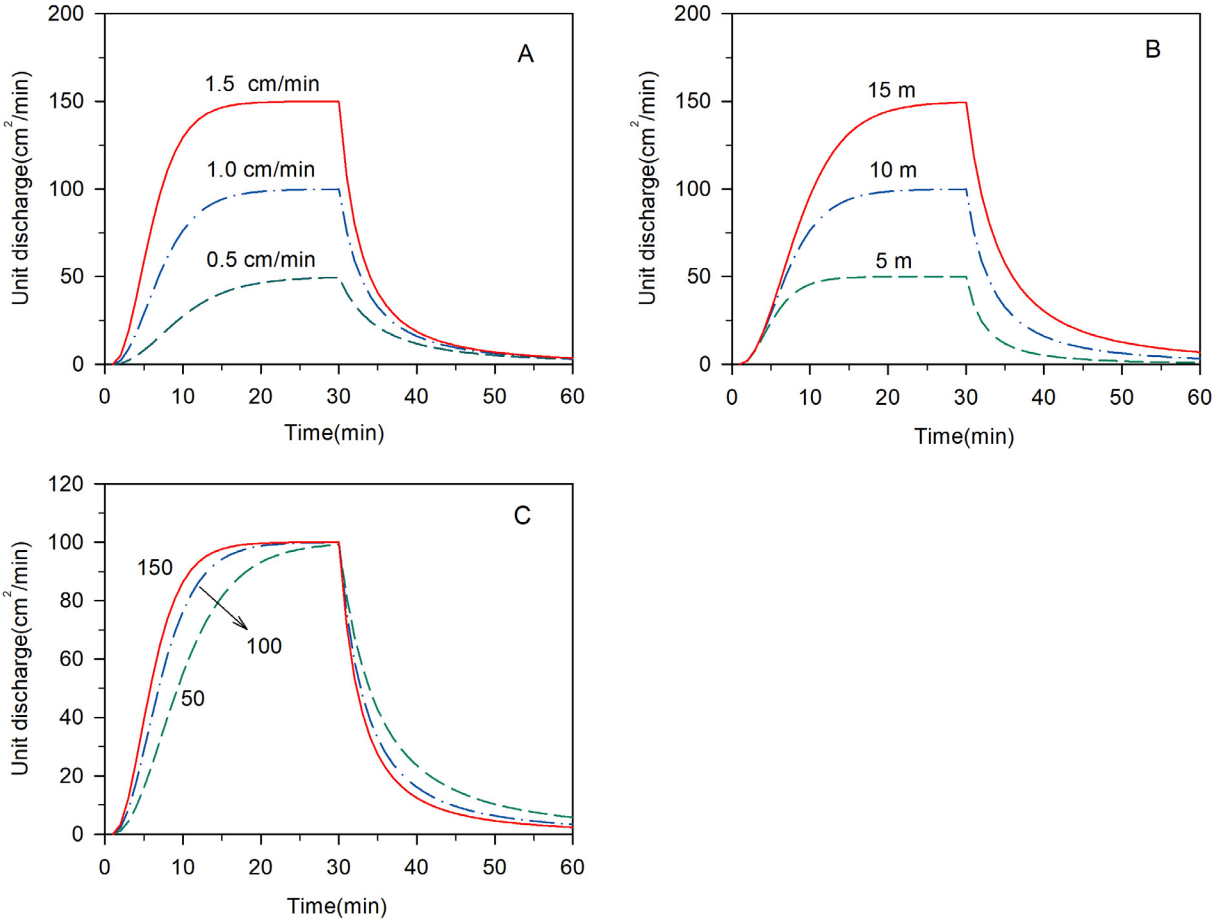

Fig. 1. Graphs of the analytical solution (runoff generation) under uniform rainfall conditions. A, B and C are the results using different rainfall intensity, slope length and parameter α, respectively.

The solution of Eq. (30) is:

$$q(x,t) = q_0\left(1+\frac{3}{2}(t-t_0)\sqrt{\frac{\alpha q_0}{L}}\right)^{-2} \tag{31}$$

The unit discharge, flow depth and the runoff amount under Case 3 condition can be expressed as:

$$Q(x,t) = q_0\left(1+\frac{3}{2}(t-t_0)\sqrt{\frac{\alpha q_0}{L}}\right)^{-2} x \tag{32}$$

$$h(x,t) = \sqrt{\frac{xq_0}{\alpha}}\left(1+\frac{3}{2}(t-t_0)\sqrt{\frac{\alpha q_0}{L}}\right)^{-1} \tag{33}$$

$$R(t) = -\frac{\frac{4}{9}\sqrt{\frac{q_0 L}{\alpha}}}{\sqrt{\frac{\alpha q_0}{L}}(t-t_0)+\frac{2}{3}} + \frac{2}{3}\sqrt{\frac{q_0 L}{\alpha}} \tag{34}$$

The following example demonstrates the analytical solution. Given continuous rainfall for 20 min over a 1000 cm long slope, at a rainfall intensity of 0.2 cm/min, decreasing to 0.1 cm/min for the next 20 min, and α assumed to be 100. Fig. 2 shows the simulated results for unit discharge, runoff depth, and runoff amount. The first rainfall stage ($0 < t < 20$) was modeled using Eqs. (22)–(24), with the second rainfall stage ($20 < t < 40$) modeled using Eqs. (27)–(29). The recession stage was modeled using Eqs. (32)–(34).

2.1.3. Comparison with another analytical solution

Cevza and Miguel (2007) described an analytical solution to the kinematic wave equation (KW) and diffusion wave equation (DW), with constant wave celerity and hydraulic diffusivity, applied to the overland flow problem. Two examples (A and B) (provided in Cevza and Miguel (2007)) were used to make a comparison, with the parameters used listed in Table 2. The simulated results of

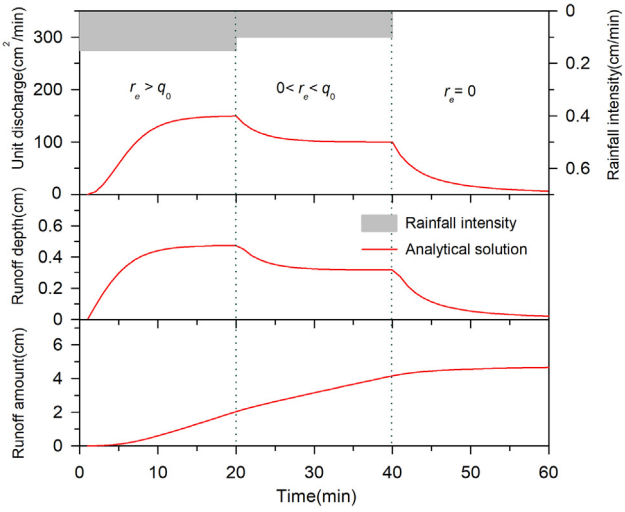

Fig. 2. Graphs of the analytical solution (runoff generation) under non-uniform rainfall conditions.

Table 2
Parameters used in the comparison of analytical solutions.

Parameters	Example A	Example B
r_e (cm/min)	0.085 ($0 < t < 30$)	0.085 ($0 < t < 3$) and 0.17 ($3 < t < 6$)
L (cm)	18,288	3048
α	444.8	165.46
t_s (min)	30	6

the solutions are listed in Fig. 3. As can be seen from the figures, there are some differences among these solutions. Comparing the curves in Fig. 3A, the results show different behaviors at peak flow and the recession stage. The KW (Cevza) reaches a maximum runoff rate for a sustained time. The KW (this study) and the DW (Cevza) have smaller peaks than given by the KW (Cevza). The KW (this study) decreases more rapidly in the recession stage than either of the KW (Cevza) and DW (Cevza). In fact, this an expected as it would then better reflect the actual situation. Fig. 3B shows the analytical solution for runoff rate under variable rainfall intensity conditions. The KW (this study) agrees reasonably well with the KW (Cevza) and DW (Cevza) for the first period of the rainfall, but not well for the second period of rainfall. The KW (this study) and DW (Cevza) have smaller and smoother peaks than the KW (Cevza). The results of the KW (this study) under variable rainfall conditions are similar to those of the DW (Cevza). Thus, the KW (this study) can better reflect the actual situation and has fewer unknown parameters (Cevza's method requires the determination of the constant celerity and hydraulic diffusivity).

2.2. Sediment transport

The process of sediment transport under rainfall conditions is usually described using the sediment continuity equation. Soil erosion on a sloped land can be divided into splash erosion and runoff erosion (Thomas and Wesley, 1994), and can be expressed as:

$$\frac{\partial(s(x,t)\cdot h(x,t))}{\partial t}+\frac{\partial(s(x,t)\cdot Q(x,t))}{\partial x}=\frac{c_f}{\rho}\gamma Jh(x,t)+\frac{c_r}{\rho}r^2 \tag{35}$$

where $s(x,t)$ is the sediment concentration (g/cm^3), γ is density of water (g/cm^3), ρ is the bulk density of soil (g/cm^3), r is the actual received rainfall intensity on unit soil surface (cm/min), c_f is the calibration constant of runoff erosion (g/min/cm^3), and c_r is the calibration constant of splash erosion (g^2·min/cm^7).

As is well known, the infiltration capacity of soil rapidly decreases at the start of rainfall, then the infiltration rate will tend to stabilize. Hence, the discharge and the runoff depth will tend to stabilize as well. This results in the erosion caused by rainfall and runoff changing very little in this stable stage. Therefore, the rate of change of sediment over time in the stable stage has been ignored in this research (Foster and Meyer, 1972; Beasley et al., 1980; Yu, 2003). Thus, Eq. (35) can be approximated as follows:

$$\frac{\partial(s(x,t)\cdot Q(x,t))}{\partial x}=\frac{c_f}{\rho}\gamma Jh(x,t)+\frac{c_r}{\rho}r^2 \tag{36}$$

2.2.1. Sediment transport under uniform rainfall conditions

The solutions for variables Q and h have been given in the previous section. Based on Eqs. (13), (14) and (36), the sediment concentration in runoff water can be expressed as:

$$s(x,t)=\frac{2\tanh\left(\frac{3}{2}\sqrt{\frac{\alpha r_e}{L}}(t-t_p)\right)c_f\gamma J\sqrt{\frac{r_e x}{\alpha}}+3c_r r^2}{3\rho r_e\tanh^2\left(\frac{3}{2}\sqrt{\frac{\alpha r_e}{L}}(t-t_p)\right)} \tag{37}$$

Combining Eqs. (12) and (37), the sediment yield rate can be expressed as:

$$S(x,t)=\frac{2c_f\gamma J}{3\rho}\tanh\left(\frac{3}{2}\sqrt{\frac{\alpha r_e}{L}}(t-t_p)\right)\sqrt{\frac{r_e x}{\alpha}}+\frac{c_r}{\rho}r^2 \tag{38}$$

where $S(x, t)$ is the sediment yield rate (g/min/cm^2).

Based on Eqs. (17), (18) and (36), the sediment concentration during the recession stage can be expressed as:

$$s_r(x,t)=\frac{1}{6}\frac{c_f\gamma J\sqrt{\frac{L}{\alpha q(t_s)}}}{\rho q(t_s)\left(\frac{3}{2}\sqrt{\frac{\alpha q(t_s)}{L}}(t-t_s)+1\right)} \tag{39}$$

where s_r(x, t) is the sediment concentration during the recession stage (g/cm^3).

Combining Eqs. (16) and (39), the sediment yield rate in recession stage can be expressed as:

$$S_r(x,t)=\frac{1}{6}\frac{c_f\gamma J\sqrt{\frac{L}{\alpha q(t_s)}}}{\rho\left(\frac{3}{2}\sqrt{\frac{\alpha q(t_s)}{L}}(t-t_s)+1\right)^3} \tag{40}$$

where S_r(x, t) is the sediment yield rate during the recession stage (g/min/cm^2).

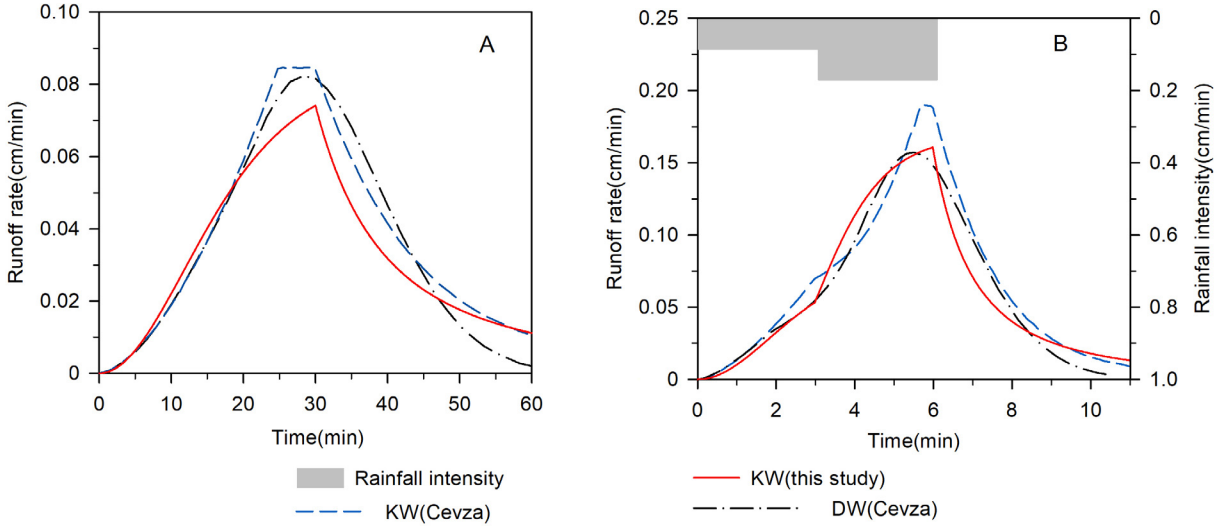

Fig. 3. Comparison of runoff rate obtained from analytical solutions in this study with the analytical solution presented by Cevza and Miguel (2007). A shows the solutions for uniform rainfall conditions; B shows the solutions for non-uniform rainfall conditions.

Integrating Eqs. (38) and (40) with respect to time yields the sediment load yield per unit area:

$$M(t)=\left(\frac{2}{3}\frac{c_f\gamma J}{\rho}\sqrt{\frac{r_e L}{\alpha}}+\frac{c_r r^2}{\rho}\right)(t-t_p)+\frac{4}{9}\frac{c_f\gamma JL}{\rho\alpha}\left(\ln\left(\exp^2\left(-\frac{3}{2}\sqrt{\frac{\alpha r_e}{L}}(t-t_p)+1\right)-\ln(2)\right)\right)\quad t\leqslant ts \tag{41a}$$

$$M(t)=\left(\frac{2}{3}\frac{c_f\gamma J}{\rho}\sqrt{\frac{r_e L}{\alpha}}+\frac{c_r r^2}{\rho}\right)(t_s-t_p)+\frac{4}{9}\frac{c_f\gamma JL}{\rho\alpha}\left(\ln\left(\exp^2\left(-\frac{3}{2}\sqrt{\frac{\alpha r_e}{L}}(t_s-t_p)+1\right)-\ln(2)\right)\right)+\frac{1}{18}\frac{c_f\gamma JL}{\alpha\rho}\left(1-\left(1+\frac{3}{2}\sqrt{\frac{\alpha q(t_s)}{L}}(t-t_s)\right)^{-2}\right)\quad t>ts \tag{41b}$$

where $M(t)$ is the sediment load per unit area (g/cm^2).

An example is given below to demonstrate the above analytical solutions of sediment transport. Again using the parameters shown in Table 1, sediment transport in the runoff was simulated for three rainfall intensities, three slope lengths and three values of parameter α (Example A, B and C). In addition, the sediment transport was also simulated for different overland slope as the parameter J appears separately in the solutions of sediment transport equations. The parameter J was specified as 0.01, 0.03 and 0.05. And the soil bulk density and Manning's roughness coefficient were specified as 1.40 g/cm^3 and 0.05 s/m$^{1/3}$, respectively. The simulated results in Fig. 4 show that the analytical solutions describe the processes of sediment transport well. As can be seen from Fig. 4, increasing rainfall intensity, slope length and overland slope result in an increase in sediment yield rate. Conversely, however, increasing values of α result in a decrease in sediment yield rate.

2.2.2. Sediment transport under natural rainfall conditions

Combining the solutions for runoff generation under natural rainfall conditions with Eq. (36). There are then three different cases to be examined.

Case 1: $r_e > q_0$. Combining Eqs. (22), (23) and (36), the solution of Eq. (36) is given by:

$$s(x,t)=\frac{2\tanh\left(\operatorname{arctanh}\left(\sqrt{\frac{q_0}{r_e}}\right)+\frac{3}{2}\sqrt{\frac{\alpha r_e}{L}}(t-t_0)\right)c_f\gamma J\sqrt{\frac{r_e x}{\alpha}}+3c_r r^2}{3\rho r_e\tanh^2\left(arctanh\left(\sqrt{\frac{q_0}{r_e}}\right)+\frac{3}{2}\sqrt{\frac{\alpha r_e}{L}}(t-t_0)\right)} \tag{42}$$

The sediment yield rate and sediment load under Case 1 condition can be expressed as:

$$S(x,t)=\frac{2c_f\gamma J}{3\rho}\tanh\left(\operatorname{arctanh}\left(\sqrt{\frac{q_0}{r_e}}\right)+\frac{3}{2}\sqrt{\frac{\alpha r_e}{L}}(t-t_0)\right)\sqrt{\frac{r_e x}{\alpha}}+\frac{c_r}{\rho}r^2 \tag{43}$$

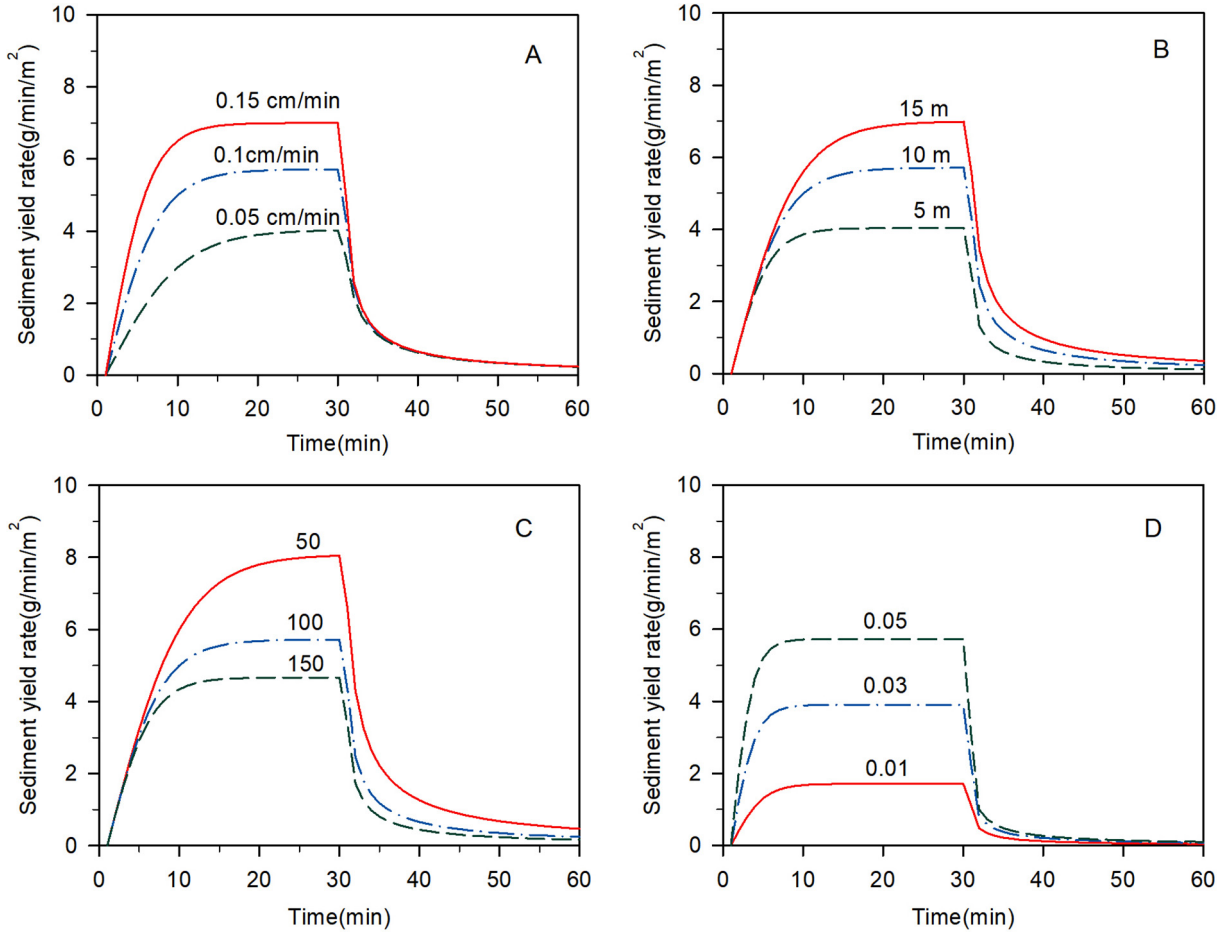

Fig. 4. Graphs of the analytical solution for sediment transport under uniform rainfall conditions. A, B, C and D are the results using different rainfall intensity, slope length, parameter α and overland slope respectively.

$$M(t)=\left(\frac{2}{3}\frac{c_f\gamma J}{\rho}\sqrt{\frac{Lr_e}{\alpha}}+\frac{c_r}{\rho}r^2\right)(t-t_0)+\frac{4}{9}\frac{c_f\gamma JL}{\rho\alpha}\left(\ln\left(\exp^2\left(-\operatorname{arctanh}\left(\sqrt{\frac{q_0}{r_e}}\right)-\frac{3}{2}\sqrt{\frac{\alpha r_e}{L}}(t-t_0)\right)+1\right)-\ln\left(\exp^2\left(-\operatorname{arctanh}\left(\sqrt{\frac{q_0}{r_e}}\right)\right)+1\right)\right) \quad (44)$$

Case 2: $0 < r_e < q_0$. Combining Eqs. (27), (28) and (36), the solution of Eq. (36) is given by:

$$s(x,t)=\frac{2\coth\left(\operatorname{arccoth}\left(\sqrt{\frac{q_0}{r_e}}\right)+\frac{3}{2}\sqrt{\frac{\alpha r_e}{L}}(t-t_0)\right)c_f\gamma J\sqrt{\frac{r_e x}{\alpha}}+3c_r r^2}{3\rho r_e\coth^2\left(\operatorname{arccoth}\left(\sqrt{\frac{q_0}{r_e}}\right)+\frac{3}{2}\sqrt{\frac{\alpha r_e}{L}}(t-t_0)\right)} \quad (45)$$

The sediment yield rate and sediment load under Case 2 condition can be expressed as:

$$S(x,t)=\frac{2c_f\gamma J}{3\rho}\coth\left(\operatorname{arccoth}\left(\sqrt{\frac{q_0}{r_e}}\right)+\frac{3}{2}\sqrt{\frac{\alpha r_e}{L}}(t-t_0)\right)\sqrt{\frac{r_e x}{\alpha}}+\frac{c_r}{\rho}r^2 \quad (46)$$

$$M(t)=\left(\frac{2}{3}\frac{c_f\gamma J}{\rho}\sqrt{\frac{Lr_e}{\alpha}}+\frac{c_r}{\rho}r^2\right)(t-t_0)+\frac{4}{9}\times\frac{c_f\gamma JL}{\rho\alpha}\left(\ln\left(\exp^2\left(-\operatorname{arccoth}\left(\sqrt{\frac{q_0}{r_e}}\right)-\frac{3}{2}\sqrt{\frac{\alpha r_e}{L}}(t-t_0)\right)-1\right)\right)-\ln\left(\exp^2\left(-\operatorname{arccoth}\left(\sqrt{\frac{q_0}{r_e}}\right)\right)-1\right) \quad (47)$$

Case3: $r_e = 0$. Combining Eqs. (32), (33) and (36), the solution of Eq. (36) is given by:

$$s(x,t)=\frac{1}{6}\frac{c_f\gamma J\sqrt{\frac{L}{\alpha q_0}}}{\rho q_0\left(\frac{3}{2}\sqrt{\frac{\alpha q_0}{L}}(t-t_0)+1\right)} \quad (48)$$

The sediment yield rate and sediment load under Case 3 condition can be expressed as:

$$S(x,t)=\frac{1}{6}\frac{c_f\gamma J\sqrt{\frac{L}{\alpha q_0}}}{\rho\left(\frac{3}{2}\sqrt{\frac{\alpha q_0}{L}}(t-t_0)+1\right)^3} \quad (49)$$

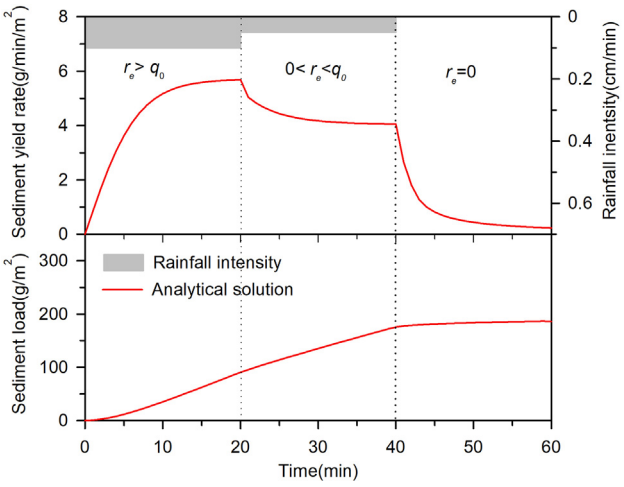

Fig. 5. Graphs of the analytical solution for sediment transport under non-uniform rainfall conditions.

$$M(t)=\frac{1}{18}\frac{c_f\gamma JL}{\alpha\rho}\left(1-\left(1+\frac{3}{2}\sqrt{\frac{\alpha q(t_0)}{L}}(t-t_0)\right)^{-2}\right) \quad (50)$$

An example follows to demonstrate the analytical solution for sediment transport under variable rainfall conditions. Given continuous rainfall for 20 min over a 1000 cm long slope, at a rainfall intensity of 0.2 cm/min, decreasing 0.1 cm/min for the next 20 min, and a value of α was assumed to be 100. Fig. 5 shows the simulated results for sediment yield rate and sediment load per unit area. The first rainfall stage ($0 < t < 20$) was modeled using Eqs. (43) and (44), with the second rainfall stage ($20 < t < 40$) modeled using Eqs. (46) and (47). The recession stage was modeled using Eqs. (49) and (50).

3. Materials and methods

3.1. Rainfall simulations

Eighty-four rainfall events (from published results; see details in Table 3) were used to verify the accuracy of our analytical solutions. These rainfall events occurred under various conditions, such as different slope lengths (from 1 to 22 m), slope gradients (from 0.02 to 0.78), soil bulk densities (from 1.20 to1.6 g/cm^3), stable infiltration rates (from 0.0045 to 0.094 cm/min), rainfall intensities (from 0.04 to 0.28 cm/min), rainfall durations (from 30 to 408 min), and Manning roughness coefficients (from 0.00004 to 0.0068 min/cm$^{1/3}$).

Rainfall events 1–3 were used to verify the analytical solution of runoff generation under uniform rainfall conditions. The experimental data were collected from Wang et al. (2015), Liu and Singh (2004), and Tao and Wu (2015), for events 1 and 3 respectively. Events 1 and 2 were conducted in the rainfall simulation hall at the State Key Laboratory of Soil Erosion and Dryland Farming on the Loess Plateau, and event 3 was carried out at the Changwu State Key Agro-Experimental Station on the Loess Plateau. The test soils were loess, rainfall intensities were 0.2, 0.16 and 0.167 cm/min, slope lengths were 5.3, 3.2 and 1 m, and soil bulk densities were 1.6, 1.35 and 1.31 g/cm^3.

Rainfall events 4–6 were used to verify the analytical solution of runoff generation under natural rainfall conditions. The experimental data were obtained from Lloyd and Tommy (2010), and the experiments were conducted in an outdoor experimental station at Nanyang Technological University. The experimental plots were 25 m long and 1 m wide, and were equipped with rainfall and flow measurement devices. The overland plane had a slope of 0.02. The three rainfall storm events used occurred between October 2002 and December 2002. The changes in rainfall intensity during natural rainfall are shown in Fig. 6.

Rainfall events 7–78 were used to determine the parameters c_f (the calibration constant of runoff erosion) and c_r (the calibration constant of splash erosion). The treatments were different slope lengths (Xing et al., 2016), different rainfall intensities (Dong et al., 2012; Zhao et al., 2015), different slope gradients (He et al., 2016; Shen et al., 2016), and different rainfall durations (Catherine et al., 2010). Five types of soil were selected for these experiments, being sandy, sandy loam, clay loam, silt loam and silt clay.

Rainfall events 79–81 were used to verify the process of sediment yield under uniform rainfall conditions. The experimental data were obtained from Zhao et al. (2015). The experiments were conducted in the simulated hall at the Red Soil Erosion and Flow Hydraulics of South China in Guangzhou City. The test used red soil taken from the non-agricultural land located in a Guangzhou suburb. Rainfall intensities used were 0.15, 0.2 and 0.3 cm/min. The slope length was 2 m, and the slope gradient was 0.42.

Table 3
List of 84 rainfall events examined in this study and the basic information of the associated hillslope.

Rainfall events	Slope length (m)	Rainfall intensity (cm/min)	Rainfall duration (min)	Slope (cm/cm)	Roughness coefficient ($min/cm^{1/3}$)	Stable infiltration rate (cm/min)	Bulk density (g/cm^3)
1 (Wang et al., 2015)	5.3	0.2	60	0.05	0.0006	0.01	1.60
2 (Tao and Wu, 2015)	1	0.167	60	0.26	0.00006	0.02	1.31
3 (Liu and Singh, 2004)	3.2	0.16	60	0.17	0.0007	0.03	1.35
4–6 (Lloyd and Tommy, 2010)	25	Fig. 6A	36	0.02	0.00004	0.01	
		Fig. 6B	27				1.57
		Fig. 6C	89				
7–21 (Xing et al., 2016)	1, 5, 10, 15, 20	0.125, 0.083, 0.042	40	0.09	0.00023	0.02	1.52
22–51 (Dong et al., 2012)	10	0.06, 0.122, 0.174,	30	0.19	0.00005	0.03	1.37
	10	0.233, 0.279		0.31	0.00007	0.05	1.22
	10			0.47	0.00011	0.04	1.27
	4.2			0.57	0.00013	0.03	1.41
	3.8			0.78	0.00014	0.04	1.24
	10			0.31	0.00009	0.02	1.66
52–55 (He et al., 2016)	5	0.15	60	0.17, 0.26, 0.34, 0.42	0.00015	0.01	1.35
56–61 (Catherine et al., 2010)	2	0.15	180	0.1, 0.2, 0.3	0.00021	0.094	1.28
		0.1	240	0.20			
		0.175	120				
		0.2	120				
62–69 (Fang et al., 2015)	5	0.15	60	0.18, 0.27, 0.36, 0.47	0.00016	0.019	1.25
		0.2	45				
70–78 (Shen et al., 2016)	10	0.08	60	0.17	0.00014	0.024	1.20
		0.13	40	0.26			
		0.17	30	0.34			
79–81 (Zhao et al., 2015)	2	0.15			0.00032	0.017	1.28
		0.2	60	0.42	0.00016	0.017	1.28
		0.3			0.00019	0.017	1.28
82–84 (Zhang et al., 2008)		Fig. 7A	408				
	22	Fig. 7B	80	0.07	0.00007	0.0045	1.26
		Fig. 7C	371				

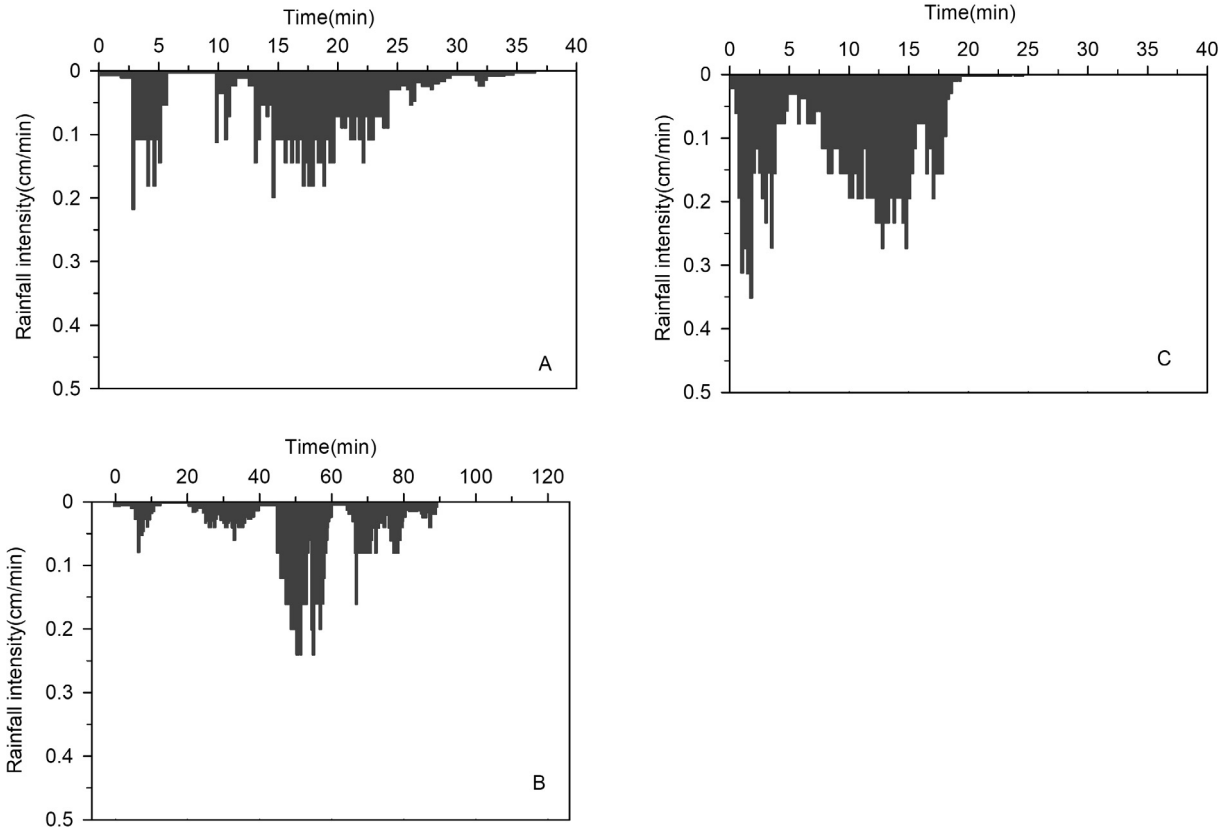

Fig. 6. The rainfall data from Lloyd and Tommy (2010). A, B and C are rainfall events 4, 5 and 6, respectively.

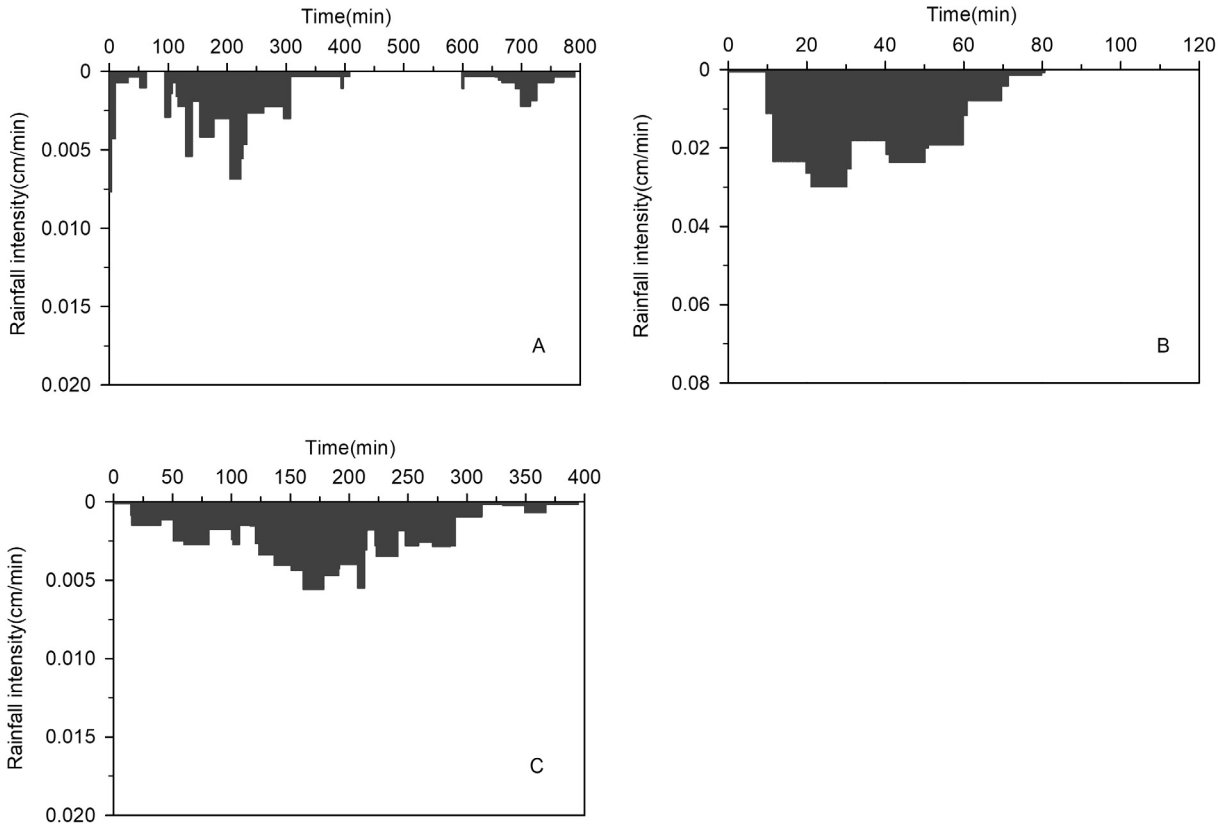

Fig. 7. The rainfall data from Zhang et al. (2008). A, B and C are rainfall events 82, 83 and 84, respectively.

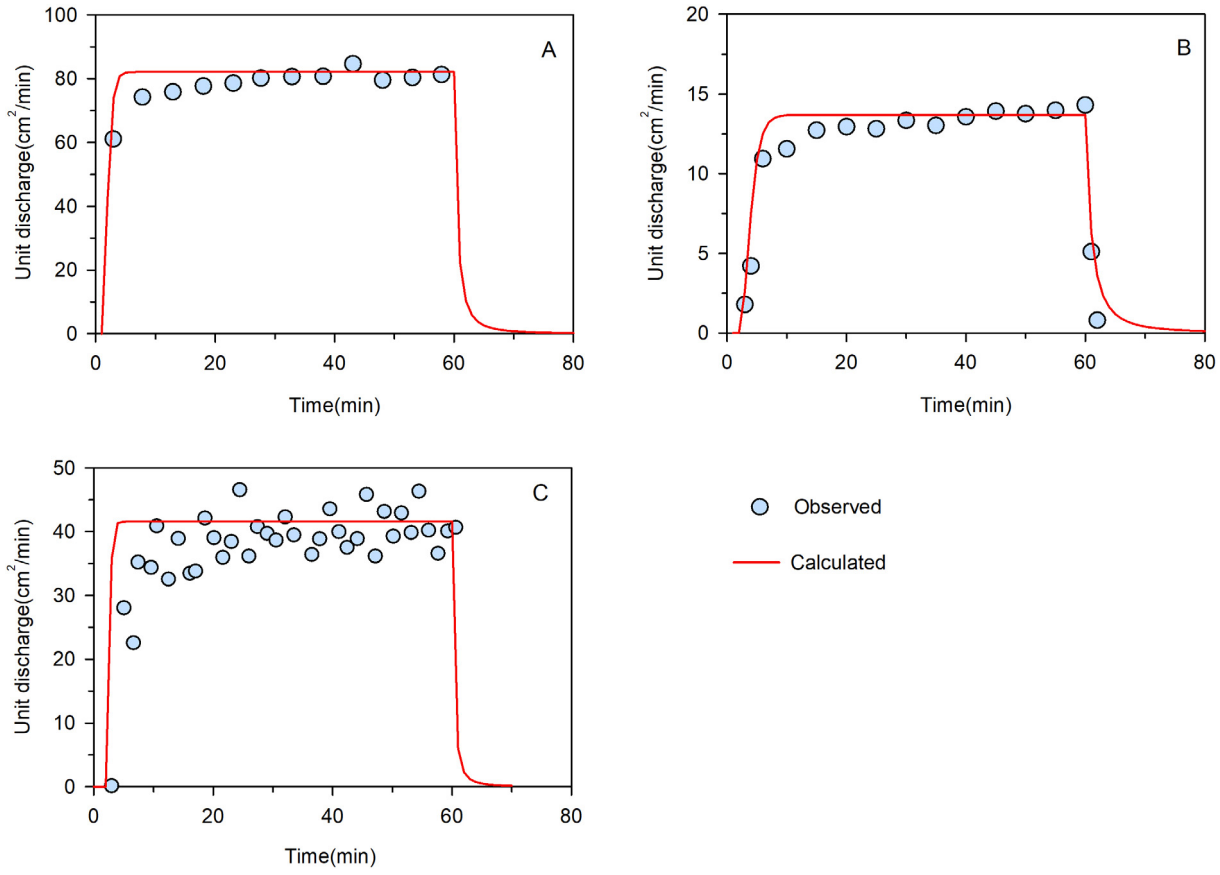

Fig. 8. Comparison of observed unit discharge with the approximated solution under uniform rainfall conditions. A, B and C are rainfall events 1, 2 and 3, respectively.

Rainfall events 82–84 were used to verify the process of sediment yield under natural rainfall conditions. The experimental data were obtained from Zhang et al. (2008). The experiments were conducted in the Soil Conservation Ecological Science and Technology Demonstration Park of Jiangxi Province. The slope grade used was 12°, and the slope length was 22 m. The testing plot was located below the uncovered slope. The changes in intensity during rainfall are shown in Fig. 7.

3.2. Data analysis

The agreement between the observed and calculated data was assessed using RMSE (root mean square error) and R^2 (Nash-Sutcliffe model efficiency coefficient):

$$RMSE = \sqrt{\frac{\sum_i^N (O_i - C_i)^2}{N}} \tag{51}$$

$$R^2 = 1 - \frac{\sum_{i=1}^N (O_i - C_i)^2}{\sum_{i=1}^N (O_i - \bar{O})^2} \tag{52}$$

where O_i is the observed data, C_i is the calculated data, N is the number of measurement, and $\bar{O}$ is the mean value of observed data.

4. Results and discussion

4.1. Overland flow

Three rainfall events (rainfall events 1–3) were used to verify the accuracy of the approximate solution under uniform rainfall conditions. The observed unit discharge was fitted with the data calculated from the approximate solution (Eqs. (13) and (17)) as shown in Fig. 8. It shows that the approximate solution overestimated the unit discharge at the initial stage but predicted well at the steady stage. The reason for the overestimated unit discharge is mainly because that the rainfall intensity was considered as being constant in the overland flow. However, rainfall events can last a long time and the soil infiltration capacity rapidly decreases during the initial stage. Hence, the approximation of the rainfall intensity may give a slightly larger runoff value than the actual one, but have no significant effect on the total runoff. The RMSE for the three rainfall events was 1.16, 0.65, and 0.93, respectively, and R^2 was 0.81, 0.92, and 0.74, respectively. It can be concluded that the approximate solution can be used to predict the unit discharge reasonably accurately.

Another three rainfall events (rainfall events 4–6) were used to verify the accuracy of the approximate solution under natural rain-

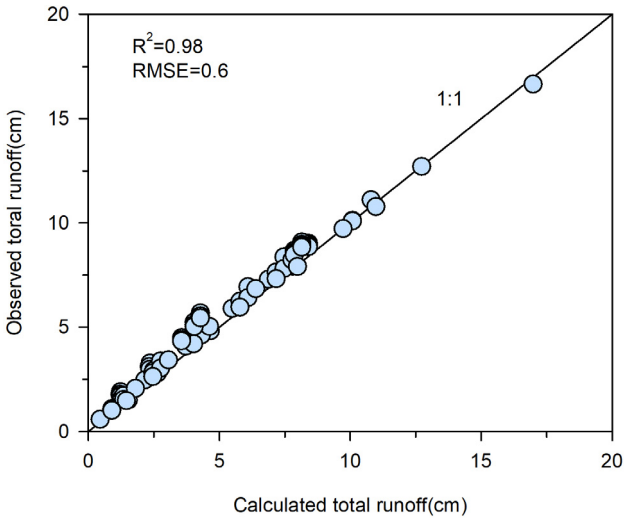

Fig. 10. Comparison of observed total runoff and calculated total runoff.

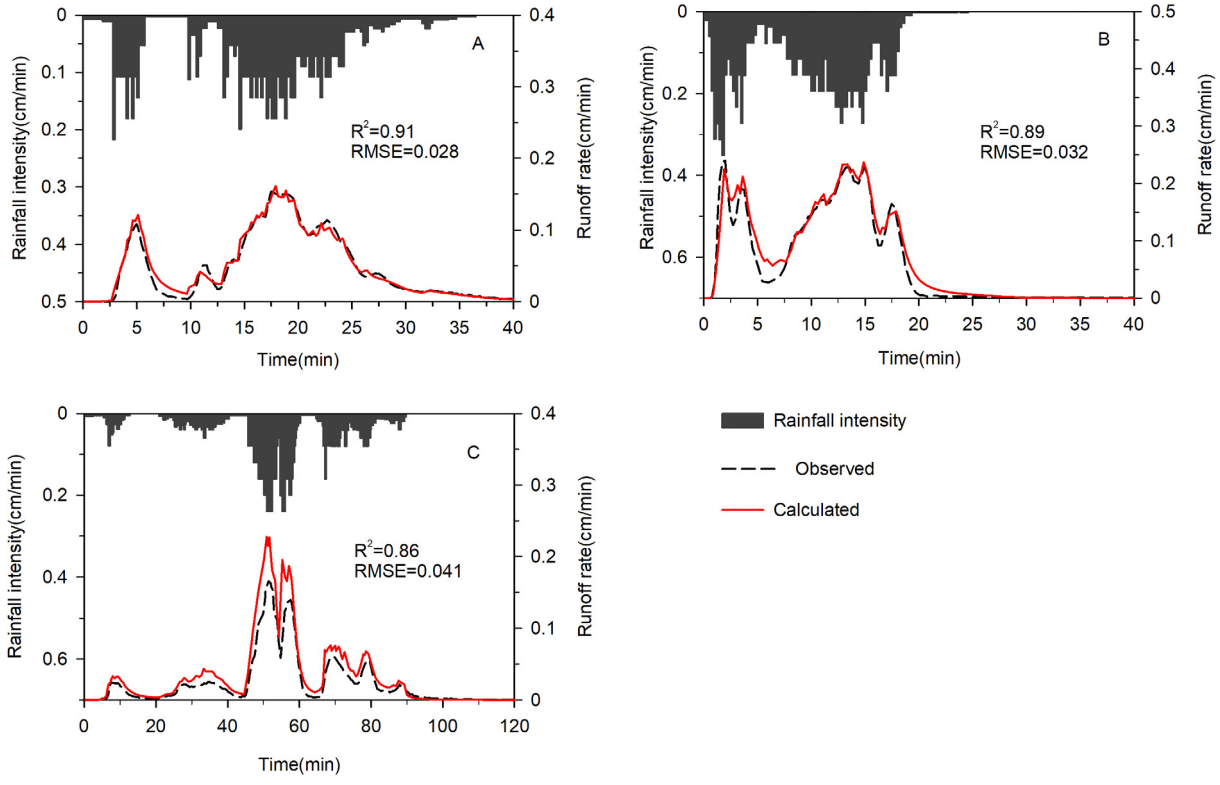

Fig. 9. Comparison of observed runoff rate with the approximated solution under natural rainfall conditions. A, B and C are rainfall events 4, 5 and 6, respectively.

fall conditions as shown in Fig. 9, which shows the observed runoff rate curve-fitted to the approximate solution (Eqs. (21), (26) and (31)). The RMSE of the three rainfall events was 0.028, 0.032, and 0.041, respectively, and the R^2 of the three rainfall events was 0.91, 0.89, and 0.86 respectively. The results indicated that the approximate solution under natural rainfall conditions can produce an accurate description of runoff generation.

Fig. 10 shows the comparison between observed total runoff and calculated total runoff. All the rainfall events were used to verify the model of total runoff. The total runoff generated under uniform conditions was calculated using Eq. (19), and the total runoff generated under natural rainfall conditions was calculated using Eqs. (24), (29) and (34). As shown in Fig. 10, almost all the points are slightly above the x = y straight line (labeled 1:1). It indicates that the calculated total runoff may slightly exceed the observed total runoff. The reason for that may be due to the model being unable to predict accurately the infiltration process in the initial stage of rainfall. The values of RMSE and R^2 are 0.6 and 0.98, respectively. Hence, the model can be used to predict the total runoff as the calculated data broadly agree with the observed data.

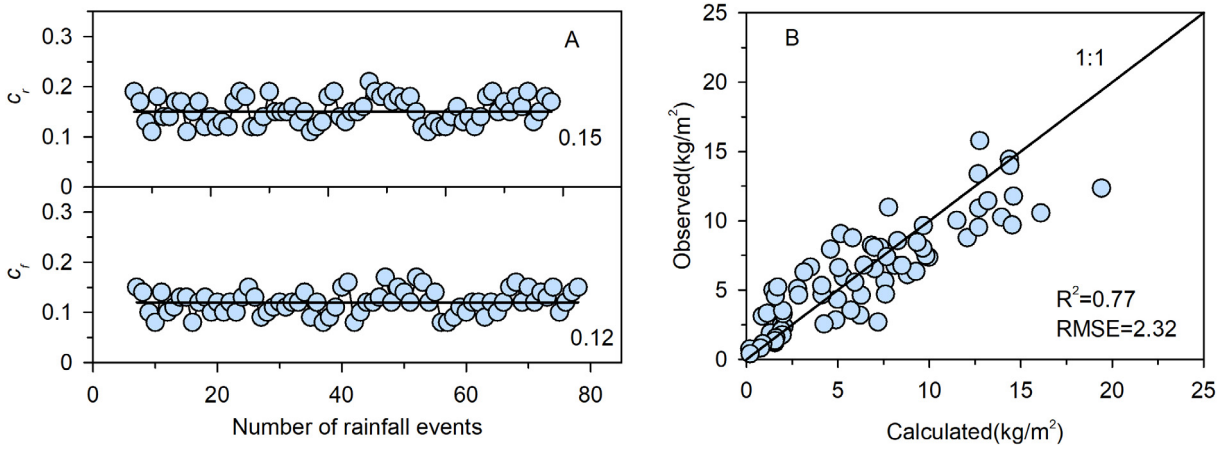

Fig. 11. The values of cr and cf obtained by fitting curves and the comparison between observed and calculated sediment yield (using the reference values for c_r and c_f).

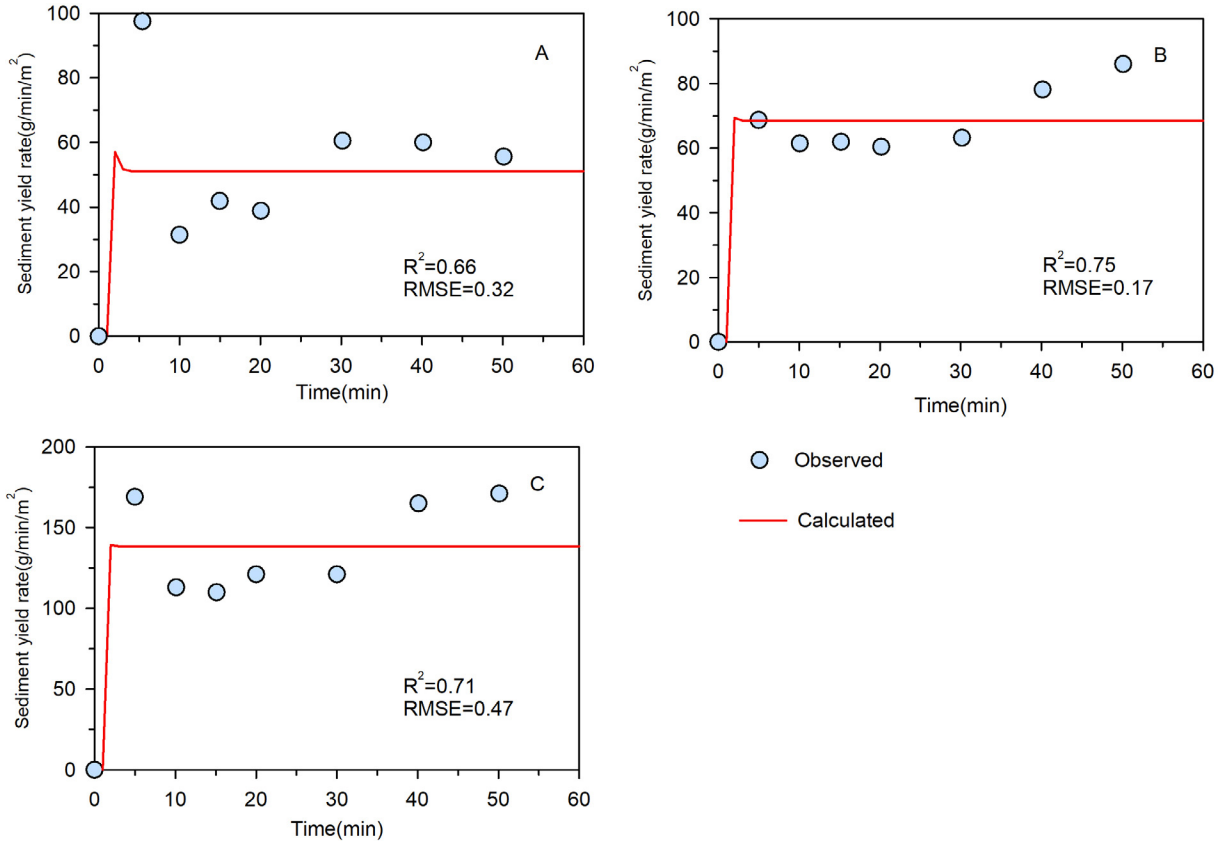

Fig. 12. Comparison of observed sediment yield rate with the approximated solution under uniform rainfall conditions. A, B and C are rainfall events 79, 80 and 81, respectively.

4.2. Sediment

4.2.1. Determination of parameters

As mentioned above, the sediment yield rate in a rainfall event under uniform rainfall conditions can be predicted with Eq. (38). However, the parameters c_r and c_f are unknown. Hence, the model cannot be easily used unless the values of c_r and c_f are defined. Seventy-two rainfall events (rainfall events 7–78) were used to determine the values of c_r and c_f. Fig. 11A shows their values that were obtained by fitting curves using Eq. (38). The results indicated that the values of c_r and c_f were different under different conditions. Overall, however, the values of c_r and c_f are within a narrow range. Hence, the mean values of c_r and c_f, 0.15 and 0.12 respectively, can be considered as recommended values that can be used to predict sediment yield. Fig. 11B shows the comparison between observed and calculated sediment yield (using the recommended values of c_r and c_f). The degree of agreement between observed data and calculated data was quantified by RMSE and R^2 (2.32 and 0.77, respectively). The results show that using recommended values does produce an error to a certain extent. The main cause of the error is that there are too many factors that affect the sediment yield but not included in the sediment continuity equation (such as water content and texture of soil surface). On the other hand, using mean values in place of actual values will also produce an error. Nevertheless, using recommended values for c_r and c_f of 0.15 and 0.12, respectively, enables the application of the proposed model much easier as well as with an acceptable accuracy.

4.2.2. Model evaluation

To verify the accuracy of the approximate solution for the sediment yield process under uniform rainfall conditions, three rainfall events (rainfall events 79–81) were used. Fig. 12 shows the comparison between observed and calculated (using Eq. (38) and the recommended values of c_r and c_f) sediment yield rate. As can be seen from Fig. 12, the approximate solution can quickly reach the stable stage after the start of rainfall, due to the change rate of sediment yield over time in the stable stage being ignored (i.e., the sediment yield only changes with distance in the stable stage). The RMSE of the three rainfall events are 6.15, 9.35, and 16.89, and the R^2 of the three rainfall events are 0.66, 0.75, and 0.71, respectively. Although the approximate solution provided in this paper may not capture the complete process during a rainfall event, it can reflect the stable value of sediment yield rate to a certain extent. The stable sediment yield rates for the three rainfall events are 54.39, 62.80 and 126.71 g/(min·m^2), and the stable values of the approximate solution are 51.14, 68.52 and 138.53 g/(min·m^2), respectively. The relative errors of the observed average sediment yield rate and stable approximate solution are 5.98%, 9.11%, and 9.41%, respectively.

Fig. 13 shows the comparison between observed sediment yield rate (rainfall events 82–84) with the approximate solution (using Eqs. (43), (46) and (49); using the recommended values of c_r and c_f) under natural rainfall conditions. The RMSE of the three rainfall events are 0.15, 0.14, and 0.13, and the R^2 of the three rainfall events are 0.86, 0.94, and 0.88, respectively. The results show that the approximate solution can closely match the observed sediment yield under natural rainfall conditions.

5. Conclusions

An approximate analytical solution for overland flow and sediment transport has been described in this paper. The obtained analytical solution was based on the assumptions that the flow regime of overland flow was transitional, with the value of parameter β (in the kinematic wave model) being approximately two, and the change rate of unit discharge with distance being constant and equal to the runoff rate at the outlet of the plane. The excess rainfall under uniform rainfall intensity conditions was treated as constant. The process of overland flow generation in the rising and recession stages can be described under uniform rainfall intensity

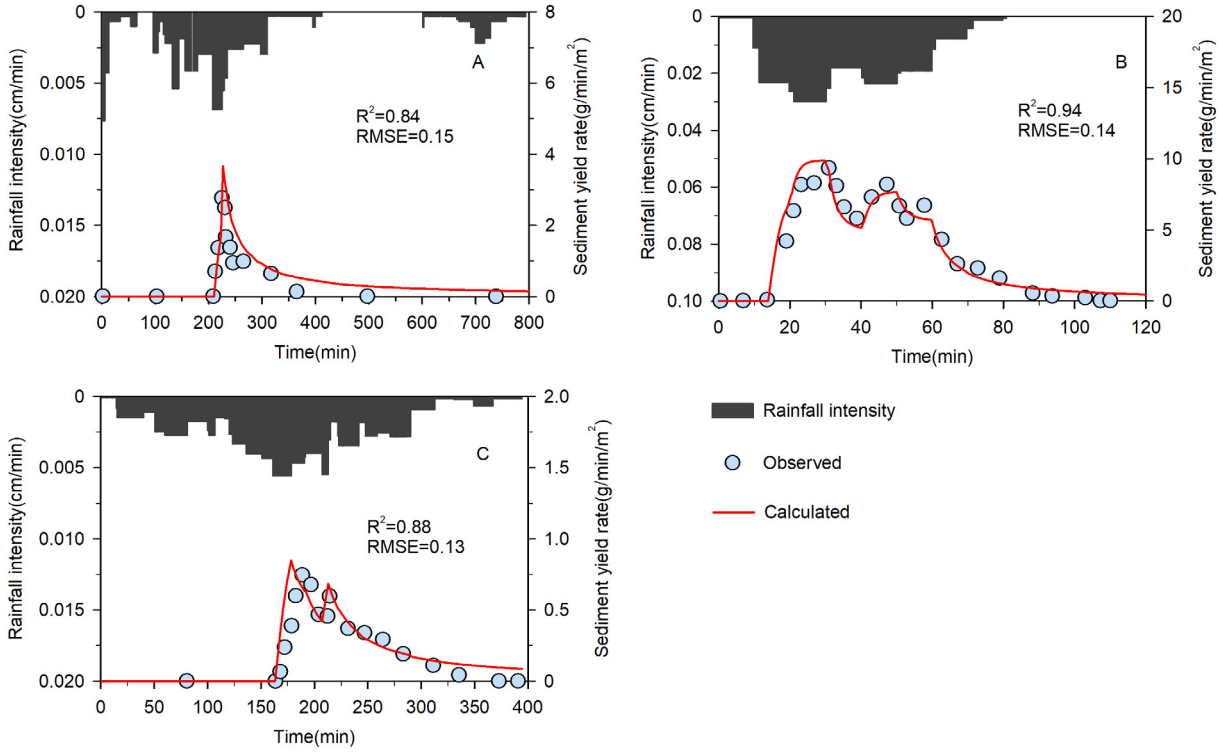

Fig. 13. Comparison of observed sediment yield rate with the approximated solution under natural rainfall conditions. A, B and C are rainfall events 82, 83 and 84, respectively.

conditions. To apply the model to natural rainfall conditions, the excess rainfall was considered as constant over a small interval $[t_0, t]$. The comparison of experimental results and calculated results shows that the formula for describing overland flow is accurate both for uniform rainfall intensity and natural rainfall conditions.

The rainfall-induced erosion was divided into splash erosion and runoff erosion. To obtain the analytical solution, the change rate of sediment with time in the stable stage was ignored. The sediment transport model was formulated for uniform rainfall conditions. The parameters c_r and c_f in the model were determined to have recommended values of 0.15 and 0.12, respectively. The comparison between experimental and calculated results shows that the approximate analytical solution (under uniform rainfall conditions) is unable to capture the complete process of sediment yield as the change rate of sediment yield with time in the stable stage was ignored in the model, but the model can accurately predict the stable value of sediment yield rate. The approximate analytical solution is sufficiently accurate when applied to natural rainfall conditions.

Acknowledgements

This study was supported by the National Natural Science Foundation of China (51239009), National Natural Science Foundation of China (05149212). We would like to thank the Editor, Associate Editor, and two reviewers for improving the quality of this paper.

References

Agnese, C., Baiamonte, G., Corrao, C., 2001. A simple model of hillslope response for overland flow generation. Hydrol. Processes 15, 3225–3238.
Beasley, D.B., Huggins, L.F., Monke, E.J., 1980. ANSWERS: a model for watershed planning. Trans. ASAE, 938–944.
Bennet, J.P., 1974. Concepts of mathematical modeling of sediment yield. Water Resour. Res. 10, 485–492.
Catherine, B., Schulze, M., Riekezapp, D., Schlunegger, F., 2010. Rill development and soil erosion: a laboratory study of slope and rainfall intensity. Earth Surf. Proc. Land. 35, 1456–1467.
Cevza, M.K., Miguel, A.M., 2007. Kinematic and diffusion waves: analytical and numerical solutions to overland and channel flow. J. Hydraul. Eng. 133, 217–228.
Crossley, A.J., Wright, N.G., Whitlow, C.D., 2003. Whitlow, local time stepping for modeling open channel flow. J. Hydraul. Eng. 129, 455–462.
Dong, J.Z., Zhang, K.L., Guo, Z.L., 2012. Runoff and soil erosion from highway construction spoil deposits: a rainfall simulation study. Transp. Res. Part D 17, 8–14.
Emmett, W.W., 1970. The Hydraulics of Overland Flow on Hillslope. United States Government Printing Office, Washington.
Fang, H.Y., Sun, L.Y., Tang, Z.H., 2015. Effects of rainfall and slope on runoff, soil erosion and rill development: an experimental study using two loess soils. Hydrol. Process. 29, 2649–2658.
Foster, G., 1986. Erosion and Sediment Transport Processes for Agricultural Watersheds. Agricultural Nonpoint Source Pollution: Model Selection and Application. Elsevier Publishing Co., New York, N.Y.
Foster, G.R., Meyer, L.D., 1972. A closed-form soil erosion equation for upland areas. In: Shen, H.W. (Ed.), Sedimentation Symposium in Honor Prof. H.A. Einstein 12. Colorado State University, Fort Collins, CO, pp. 1–12.19.
Gottardi, G., Venutelli, M., 2008. An accurate time integration method for simplified overland flow models. Adv. Water Resour. 31, 173–180.
Govindaraju, R.S., Jones, S.E., Kavvas, M.L., Kawas, M.L., 1988. On the diffusion wave model for overland flow: 1. Solution for steep slopes. Water Resour. Res. 24, 734–744.
Hayami, S., 1951. On the propagation of flood waves. Disaster Prev. Res. Inst. 1, 45–46.
He, J.J., Sun, L.Y., Gong, H.L., Cai, Q.G., Jia, L.J., 2016. The characteristics of rill development and their effects on runoff and sediment yield under different slope gradients. J. Mountain Sci. 13, 397–404.
Henderson, F.M., Wooding, R.A., 1964. Overland flow and groundwater flow form a steady rainfall of finite duration. J. Geophys. Res. 69, 1531–1540.
Horton, R.E., 1938. The interpretation and application of runoff plane experiments with reference to soil erosion problems. Soil Sci. Soc. Am. Proc. 1, 401–437.
Kazeyilmaz-Ahan, C.M., Medina, M.A., 2007. Kinematic and diffusion waves: analytical and numerical solutions to overland and channel flow. J. Hydraul. Eng. 133, 217–228.
Kazeyilmaz-Ahan, C.M., 2012. An improved solution for diffusion waves to overland flow. Appl. Math. Model. 36, 4165–4172.
Lackey, T.C., Sotiropoulos, F., 2005. Role of artificial dissipation scaling and multigrid acceleration in numerical solutions of the depth-averaged free-surface flow equations. J. Hydraul. Eng. 131, 755–769.
Liu, Q.Q., Singh, V.P., 2004. Effect of microtopography, slope length and gradient, and vegetation cover on overland flow through simulation. J. Hydrol. Eng. 9, 375–382.
Lloyd, H.C., Tommy, S.W., 2010. Improving event-based rainfall-runoff modeling using a combined artificial neural network-kinematic wave approach. J. Hydrol. 390, 92–107.
Luce, C.H., Cundy, T.W., 1992. Modification of the kinematic wave-Philip infiltration overland flow model. Water Resour. Res. 28, 1179–1186.
Mizumura, K., 2006. Analytical solutions of nonlinear kinematic wave model. J. Hydrol. Eng. 11, 539–546.
Moore, I.D., 1985. Kinematic overland flow: generalization of Rose's approximate solution. J. Hydrol. 82, 233–245.
Morgan, R.P.C., Quinton, J.N., Smith, R.E., Gover, G., Poesen, K., Auerswald, K., Chisci, G., Torri, D., Styczen, M.E., 1998. The European soil erosion model (EUROSEM): a dynamic approach for predicting sediment transport from fields and small catchments. Earth Surf. Proc. Land. 23, 527–544.
Morooka, Y., Cheng, D., Yoshimi, K., Wang, C.W., Yamada, T., 2016. Proposal and application of a new theoretical framework of uncertainty estimation in rainfall runoff process based on the theory of stochastic process. Proc. Eng. 154, 589–594.
Nearing, M., Foster, G., Lande, L., Finknear, S., 1989. A process-based soil erosion model for usda-water erosion prediction project technology. Trans. ASAE 32, 1587–1593.
Parlange, J.Y., Rose, C.W., Sander, G., 1981. Kinematic flow approximation of runoff on a plane: an exact analytical solution. J. Hydrol. 52, 171–176.
Raff, D.A., Ramirez, J.A., 2005. A physical, mechanistic and fully coupled hillslope hydrology model. Int. J. Numer. Methods Fluids 49, 1193–1212.
Rao, S.G., Kavvas, M.L., 1991. Modelling the erosion process over steep slopes: approximate analytical solutions. J. Hydrol. 127, 279–305.
Sander, G.C., Parlange, J.Y., Hogarth, W.L., Haverkamp, R., 1990. Kinematic flow approximation to runoff on a plane: solution for infiltration rate exceeding rainfall rate. J. Hydrol. 113, 193–206.
Sander, G.C., Rose, C.W., Hogarth, W.L., Parlange, J.Y., Lisle, I.G., 2014. Mathematical soil erosion model. Treatise Geomorphol. 16, 228–258.
Shen, H.O., Zheng, F.L., Wen, L.L., Han, Y., Hu, W., 2016. Impacts of rainfall intensity and slope gradient on rill erosion processes at loessial hillslope. Soil Tillage Res. 155, 429–436.
Singh, V.P., 2002. Is hydrology kinematic? Hydrol. Process. 16, 667–716.
Tao, W.H., Wu, J.H., 2015. Study on numerical simulation of slope runoff and sediment yield rule. J. Soil Water Conserv. 30, 54–57.
Tsai, T.L., Yang, J.C., 2005. Kinematic wave modeling of overland flow using characteristics method with cubic-spline interpolation. Adv. Water Resour. 28, 661–670.
Thomas, W.H., Wesley, P.J., 1994. Predicting sediment yield in storm-water from urban areas. J. Water Resour. Panning Manage. 120, 630–650.
Wang, H., Gao, J.E., Zhang, M.J., Li, X.H., Zhang, S.L., Jia, L.Z., 2015. Effects of rainfall intensity on groundwater recharge based on simulated rainfall experiments and a groundwater flow model. Catena 127, 80–91.
Wang, G.T., Chen, S., Boll, J., 2002. Modelling overland flow based on Saint-Venant equations for a discretized hillslope system. Hydrol. Process. 16, 2409–2421.
Wang, A., Jin, C., Liu, J., Pei, T., 2006. A modified Hortonian overland flow model based on laboratory experiments. Water Resour. Manage. 20, 181–192.
Xing, W.M., Yang, P.L., Ren, S.M., Ao, C., Li, X., Gao, W.H., 2016. Slope length effects on process of total nitrogen loss under simulated rainfall. Catena 139, 73–81.
Yu, B., 2003. A Unified framework for water erosion and deposition equations. Soil Sci. Soc. Am. J. 67, 251–257.
Ying, X.Y., Abdul, A.K., Sam, S.Y.W., 2004. Upwind conservative scheme for the Saint Venant equations. J. Hydraul. Eng. ASCE 130, 977–987.
Zhao, Q.H., Li, D.Q., Zhuo, M.N., Xie, Z.Y., 2015. Effect of rainfall intensity and slope gradient on erosion characteristics of the red soil slope. Stoch. Environ. Res. Risk Assess. 29, 609–621.
Zhang, Z.Y., Zhang, G.H., Zuo, C.Q., Pi, X.Y., 2008. Hillslope soil erosion and runoff model for natural rainfall events. Acta Mech. Sin. 24, 277–283.